

Controlling the conductance of molecular junctions using proton transfer reactions:

A theoretical model study

Chriszandro Hofmeister, Pedro B. Coto, and Michael Thoss¹

Institut für Theoretische Physik und Interdisziplinäres Zentrum für Molekulare Materialien

Friedrich-Alexander-Universität Erlangen-Nürnberg

Staudtstr. 7/B2, D-91058 Erlangen, Germany

The influence of an intramolecular proton transfer reaction on the conductance of a molecular junction is investigated employing a generic model, which includes the effects of the electric field of the gate and leads electrodes and the coupling to a dissipative environment. Using a quantum master equation approach it is shown that, depending on the localization of the proton, the junction exhibits a high or low current state, which can be controlled by external electric fields. Considering different regimes, which range from weak to strong hydrogen bonds in the proton transfer complex and comprise situations with high and low barriers, necessary preconditions to achieve control are analyzed. The results show that systems with a weak hydrogen bond and a significant energy barrier for the proton transfer can be used as molecular transistors or diodes.

I. INTRODUCTION

The field of molecular-scale electronics has seen tremendous progress in recent years, both with respect to experimental investigations and theoretical studies of the underlying transport mechanisms.¹⁻⁶ The most widely studied architecture in this field is a molecular junction, where a single molecule is bound to metal or semiconductor electrodes. Molecular junctions provide interesting systems to study basic mechanisms of non-equilibrium charge transport in a many-body quantum system at the nanoscale. An intriguing question concerns the possibility to realize the functionality of an electronic device with a single molecule in a molecular junction. The theoretical proposal of a molecular rectifier several decades ago⁷ can be considered as a starting point of the field. In recent years, experimental studies have shown that the current-voltage characteristics of molecular junctions may resemble those of basic electronic devices, such as rectifiers⁸⁻¹⁰ or transistors.^{11,12} An important element for the design of molecular memory or logic devices is a molecular switch.¹³ A molecular junction may be used as a nanoswitch, if the molecule can exist in two or more differently conducting states that are sufficiently stable and can be reversibly transferred into each other.

A variety of different mechanisms have been proposed to achieve reversible switching of molecular junctions between different conductance states.¹³⁻²¹ Most mechanism for optical switches considered so far are based on light-induced conformational changes, in particular isomerization reactions,^{19,20} or ring-opening reactions^{16,17} of the molecular bridge. Nonoptical mechanisms include reversible redox reactions, for example, in catenane and rotaxane molecules triggered by voltage pulses.¹⁸

As an alternative mechanism for switching of molecular junctions, hydrogen tautomerization or proton transfer reactions have been proposed recently.²¹⁻²⁴ Employing STM experiments, it was demonstrated that naphthalocyanine molecules at Cu(110)²¹ and porphyrin at Ag(111)²⁴ show current-induced switching, which is caused by hydrogen transfer. Moreover, photoinduced excited state hydrogen transfer was proposed as a mechanism to switch molecular junctions.²² Simulations show that this mechanism is also active in molecular junctions that use carbon nanotubes as electrodes.²⁵ In contrast to other mechanisms suggested previously to realize molecular switches, hydrogen (or proton) translocation within the molecular bridge has the advantage that the overall length and thus the molecule-electrode binding geometry of the junction is not changed significantly. This makes this mechanism a promising candidate for a molecular switch.

In previous work,²⁶ we have shown that a proton transfer reaction triggered by an external

electrostatic field provides another possibility to control the conductance state of a molecular junction. A prototype example is the reaction depicted in Fig. 1, which involves proton transfer between a nitrogen and an oxygen center in a hydrogen-bonding complex. Similar results have been reported also for different systems.²⁷

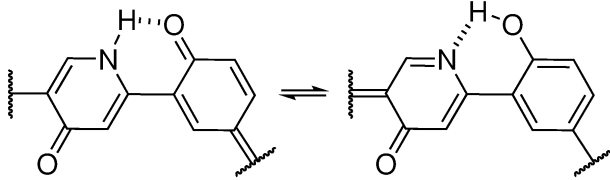


Figure 1. Scheme of an intramolecular proton transfer reaction triggered by an external electrostatic field. The tautomers exhibit distinctive conductance properties as a consequence of their different electronic structure.

So far, our studies of proton transfer in molecular junctions considered the conductance for nuclei fixed at the geometry of the enol or keto tautomer. A complete description requires to incorporate the coupling of the electrons to the motion of the proton in the junction at finite bias voltage, which is a challenging nonequilibrium transport problem. The theoretical description is further complicated by the fact that the large amplitude motion of the proton requires a potential beyond the harmonic approximation. As a consequence, theoretical approaches which rely on the harmonic approximation for the vibrational degrees of freedom cannot be used. In the present paper, we use a generic model with parameters motivated by our previous first-principles studies²⁶ and employ a quantum master equation at the level of Redfield theory to tackle this problem. Similar approaches, sometimes combined with classical approximations or inelastic scattering theory, have been used before to investigate transport in molecular junctions involving large amplitude motion.^{28–34} Based on this methodology, we analyze the transport properties and show that the conductance state of a molecular junction can indeed be controlled using a proton transfer reaction. Thereby, we consider both the influence of gate and bias voltages on the motion of the proton. Depending on the specific realization and parameters, the current-voltage characteristics of the junction can resemble those of a diode or a transistor.

The paper is organized as follows: After an introduction of the model in Sec. II, we outline the theoretical methodology in Sec. III. The results are presented in Sec. IV, divided into two parts. In the first part, we consider a system with a weak hydrogen bond in the proton

transfer complex corresponding to a high barrier. In the second part, we discuss results for systems with stronger hydrogen bonding. Sec. V summarizes and concludes.

II. MODEL

To study the influence of an intramolecular proton transfer process on the conductance of a molecular junction we consider a model described by the Hamiltonian

$$H = H_S + H_L + H_B + H_{SL} + H_{SB}, \quad (1)$$

where H_S corresponds to the molecule (in the following also referred to as the system), H_L to the left and right leads and H_B represents a dissipative environment. The coupling of the molecule to the leads and the environment are denoted by H_{SL} and H_{SB} , respectively, and taken together define the system-reservoir coupling $H_{SR} = H_{SL} + H_{SB}$.

The Hamiltonian of the system, H_S , describes not only the electronic states of the molecule but it also accounts for the motion of the proton. In our model, we consider a single electronic state of the molecule (the bridge state) in the basis defined by the neutral and charged state of the molecule, $(|0\rangle)$ and $(|1\rangle)$, respectively. Denoting the corresponding Hamiltonian elements by h_0 and h_1 , respectively, H_S can be expressed as

$$H_S = h_0 d d^\dagger + h_1 d^\dagger d, \quad (2)$$

where d^\dagger and d are the fermionic creation and annihilation operators. The Hamiltonian elements take the form

$$h_i = -\frac{1}{2M} \frac{\partial^2}{\partial x^2} + V_i(x), \quad (3)$$

where M denotes the mass of the proton.

The potential of the neutral state is given by $V_0(x) = V(x) + V_{\text{ext}}(x)$ where $V(x)$ is the potential for the intramolecular motion of the proton and $V_{\text{ext}}(x)$ accounts for the influence of external fields, in the present case the gate and the leads electric potentials. To describe the motion of the proton between the donor (D) and acceptor (A) moieties (cf. Fig. 2), we use a double-well potential given by

$$V(x) = \frac{\varepsilon_d}{2l}(x+l) + \frac{V_b - 0.5\varepsilon_d}{l^4}(x+l)^2(x-l)^2, \quad (4)$$

where the minima of the potential are separated by a distance $x_T = 2l$ and the energy of the right well is detuned with respect to that of the left by ε_d to account for the general

non-symmetrical case where the donor and acceptor states have different stabilities.²⁶ In Eq. (4), $V_b = V(0)$ denotes the potential energy at $x = 0$, i.e. the maximum of the double-well potential, and is in the following referred to as the barrier energy of the proton transfer process (see Fig. 3 for a schematic representation). In general, this potential may be different in the neutral and charged state of the molecule. Here we assume for simplicity that upon charging, the potential only acquires a constant shift given by the electron affinity ϵ_0 yielding $V_1(x) = V_0(x) + \epsilon_0$ for the potential of the charged state. In the calculations reported below a value of $\epsilon_0 = 0.1$ eV is chosen. The effect of changes of the form of the potential upon charging on the transport properties will be considered in future work.

The distances ($2l$) between the minima of the double-well potential employed in the simulations have been selected to characterize different hydrogen bond situations. Employing the acceptor (A) proton distance in the donor state, $d_D(AH)$, a hydrogen bond is considered weak for $d_D(AH) > 2.0$ Å and strong for $d_D(AH) < 1.5$ Å.^{35–37} Accordingly, in this work we have considered three sets of parameters (see Table I) corresponding to weak, medium and strong hydrogen bonding regimes. In addition, for simplicity, the equilibrium bond distances $d(DH)$ and $d(AH)$ in both the donor and acceptor states have been taken as $d(DH) = d(AH) = 1.0$ Å. Using these values, the translocation length of the proton is given by the relation $x_T = d_D(AH) - d(DH)$. An aspect that strongly affects the transport properties is the height of the barrier of the double-well potential. In this work, we have considered the situation where the system with weak hydrogen bonding exhibits a significant barrier while the other two systems have rather small or vanishing barriers.

The effects of the external field of the gate and source/drain electrodes on the motion of the proton depend in principle on the specific nature of the chemical species involved in the process. To account for these effects in our simulations we use a simplified model that is based on the direction of the transfer path of the proton between the donor and acceptor moieties (see Fig. 2). The direction determined by the angle ϕ characterizes the influence of the electric fields of the gate and the lead electrodes (which are assumed to be perpendicular) and is described by the external electrostatic potential $V_{\text{ext}} = -Ex$ with

$$E = - \left(\frac{U_g}{d} \sin(\phi) + \frac{U_b}{L_m} \cos(\phi) \right), \quad (5)$$

where U_b and U_g are the bias and the gate voltage, respectively, L_m is the length of the molecular bridge, and d is the distance between the gate electrode and the junction. In the simulations reported below, we have used $L_m = d = 1$ nm.

In our model, the left (l) and right (r) leads are described by reservoirs of noninteracting

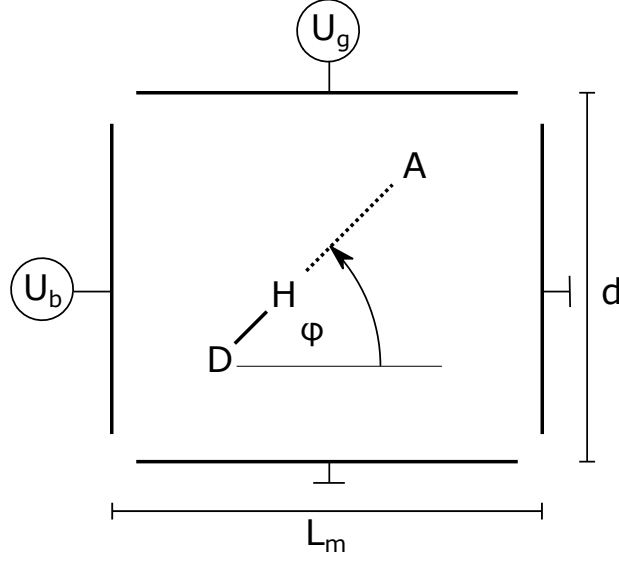


Figure 2. Schematic representation of the proton transfer model system investigated in this work. The angle between the transfer path and the bias field tuned by U_b is denoted with ϕ . The bias field is perpendicular to the gate field tuned by U_g .

electrons,

$$H_L = \sum_{\alpha \in r, l} \sum_{k_\alpha} \epsilon_{k_\alpha} c_{k_\alpha}^\dagger c_{k_\alpha}, \quad (6)$$

where c_{k_α} and $c_{k_\alpha}^\dagger$ denote the creation and annihilation operators for an electron with energy ϵ_{k_α} in the k -th state of lead α . In equilibrium, the occupation of the lead states is given by the Fermi distribution $f_\alpha(\epsilon) = 1 / (1 - \exp[\beta(\epsilon - \mu_\alpha)])$ where $\beta = 1 / k_B T$ and μ_α is the chemical potential of the lead. The temperature of the reservoirs is set to $T = 293$ K for all calculations presented in this work. For finite bias voltage U_b , we assume a symmetric shift of the chemical potentials, $\mu_{l,r} = \pm \frac{U_b}{2}$, with respect to the Fermi level at $\epsilon_f = 0$ eV.

The molecule-lead interaction is described by

$$H_{SL} = \sum_{\alpha \in l, r} \sum_{k_\alpha} V_{k_\alpha} s(x) (d^\dagger c_{k_\alpha} + c_{k_\alpha}^\dagger d). \quad (7)$$

Thereby, the molecule-lead coupling strengths V_{k_α} and the electronic energies ϵ_{k_α} are defined by the level-width function $\Gamma_\alpha(E) = 2\pi \sum_{k_\alpha} |V_{k_\alpha}|^2 \delta(E - \epsilon_{k_\alpha})$. In this work, we consider the leads to be semi-infinite chains described by a tight-binding model,^{38,39} which implies

$$\Gamma_\alpha(E) = \begin{cases} \frac{\nu^2}{\gamma^2} \sqrt{4\gamma^2 - (E - \mu_\alpha)^2} & |E| \geq 2|\gamma| \\ 0 & |E| < 2|\gamma| \end{cases} \quad (8)$$

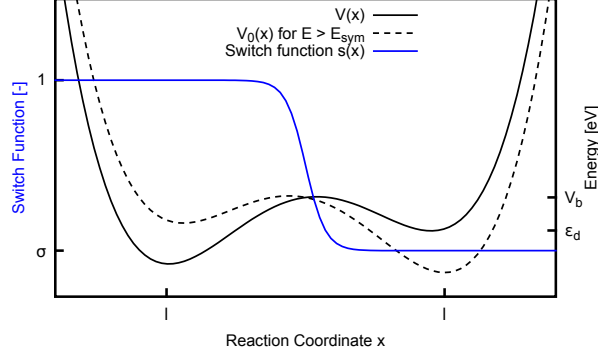


Figure 3. Potentials used to model the intramolecular proton transfer reaction with the parameters barrier energy V_b , detuning energy ϵ_d , and distance of the minima $2l$ defining the translocation length x_T . $V(x)$ is the potential without external fields, while $V_0(x)$ includes an external field of the gate electrode (shown for a value of $E > E_{sym}$). The switch function $s(x)$ scales the molecule-lead coupling depending on the location of the proton.

The parameters γ and ν in $\Gamma_\alpha(E)$, describing the coupling strength between two neighboring sites in the leads and between the molecule and the leads, respectively, are set to $\gamma = 3$ eV and $\nu = 0.1$ eV corresponding to a weak molecule-lead coupling and a band width of 6 eV.

To model the dependence of the conductance on the position of the proton, we introduce a dimensionless switch function

$$s(x) = \frac{1 + \sigma}{2} - \frac{1 - \sigma}{2} \tanh(x), \quad (9)$$

which effectively reduces the coupling matrix elements V_{k_α} by the factor σ when the proton is localized in the right potential well. In the calculations presented below, a value of $\sigma = 0.1$ is used. As a result (see below), the conductance is larger (“ON” state) for a proton located in the left well and smaller (“OFF” state) in the right well. In addition, depending on the strength of the external electric field E , the global minimum of the potential may be tuned from the left to the right well, as illustrated in Fig. 3.

In a molecular junction the motion of the proton is coupled to other vibrational degrees of freedom of the molecular bridge as well as to phonons in the leads, which may cause energy relaxation. To model this effect, we consider the coupling of the proton to a reservoir of harmonic oscillators,

$$H_B = \sum_j \omega_j b_j^\dagger b_j, \quad (10)$$

where b_j^\dagger and b_j are the creation and annihilation operators of the harmonic oscillator with frequency ω_j and assume that the proton couples linearly to the oscillators of the reservoir,

$$H_{SB} = \sum_j \lambda_j q_j x, \quad (11)$$

where $q_j = (b_j + b_j^\dagger)/\sqrt{2}$ denotes the coordinate of the j th bath oscillator. The individual coupling strengths λ_j are characterized by the bath spectral density given by $J(\omega) = \sum_j \lambda_j^2 \delta(\omega - \omega_j)$. In this work, we use an Ohmic bath with spectral density

$$J(\omega) = \eta \omega e^{-\frac{\omega}{\omega_c}}. \quad (12)$$

The maximum of the spectral density is given by the characteristic frequency, $\omega_c = 0.097$ eV, and the parameter η defines the overall coupling strength (see below).

| System | Weak | Medium | Strong |
|-------------------|-------------|---------------|---------------|
| $d_D(AH)$ (Å) | 2.5 | 2.0 | 1.5 |
| l (Å) | 0.75 | 0.50 | 0.25 |
| V_b (eV) | 0.8 | 0.2 | 0.025 |
| ϵ_d (eV) | 0.3 | 0.1 | 0.05 |

Table I. Parameter sets for the three systems considered corresponding to weak, medium, and strong hydrogen bonding regimes.

III. METHODOLOGY

We treat the molecular junction in the framework of open quantum systems, where the molecule is the system of interest. The reduced density matrix of the molecule, ρ , is defined by tracing over the reservoir degrees of freedom, $\rho = \text{Tr}_R(\varrho)$, where ϱ denotes the density matrix of the overall system. The dynamics of the reduced density matrix is described employing a Markovian quantum master equation in the weak coupling limit, also known as Redfield equations^{40,41} given by

$$\frac{\partial \rho}{\partial t} = \mathcal{L}\rho(t) = \mathcal{L}_S \rho(t) + \mathcal{R}\rho(t). \quad (13)$$

Thereby, the Liouvillian superoperators read

$$\begin{aligned} \mathcal{R}\rho(t) &= -\text{Tr}_R \int_0^\infty d\tau [H_{SR}, [H_{SR}(-\tau), \rho(t) \otimes \rho_R]], \\ \mathcal{L}_S \rho(t) &= -i [H_S, \rho(t)], \end{aligned} \quad (14)$$

where $H_{SR}(\tau) = e^{-i(H_S+H_L+H_B)\tau} H_{SR} e^{i(H_S+H_L+H_B)\tau}$ is the molecule-reservoir interaction transformed to the interaction picture.

Employing the eigenstates of H_S , $\{|m, i\rangle\}$, where $|m, 0\rangle$ denotes the vibrational states of the neutral molecule, i.e. the eigenstates of h_0 , and $|m, 1\rangle$ those of the charged molecule (h_1), Eq. (13) reads

$$\dot{\rho}_{mn}^{jk} = \sum_{l,\mu\nu} \mathcal{L}_{S mn,\mu\nu}^{jl} \rho_{\mu\nu}^{lk} + \mathcal{R}_{mn,\mu\nu}^{jl} \rho_{\mu\nu}^{lk}, \quad (15)$$

where we use the notation $\rho_{mn}^{jk} = \langle m, j | \rho | n, k \rangle$. The operator \mathcal{L}_S governs the free time evolution of the molecule in absence of the reservoirs and is given by

$$\mathcal{L}_S^{00}{}_{n'_1 n'_2, n_1 n_2} = i \delta_{n'_2 n_2} \delta_{n'_1 n_1} (E_{n_2}^0 - E_{n_1}^0) \quad (16a)$$

$$\mathcal{L}_S^{11}{}_{v'_1 v'_2, v_1 v_2} = i \delta_{v'_2 v_2} \delta_{v'_1 v_1} (E_{v_2}^1 - E_{v_1}^1). \quad (16b)$$

The relaxation operator \mathcal{R} describes the interaction with the reservoirs including the leads and the harmonic bath, $\mathcal{R} = \mathcal{R}_L + \mathcal{R}_B$. Thereby, the initial state of the reservoir is assumed to be a product state $\rho_R = \rho_L \rho_B$ with the initial density matrix of the leads

$$\rho_L = \exp(-\beta H_L - \sum_{\alpha \in \{l, r\}} \mu_\alpha \sum_{k_\alpha} c_{k_\alpha}^\dagger c_{k_\alpha}) \quad (17)$$

and for the harmonic bath $\rho_B = \exp(-\beta H_B)$. In the $\{|m, i\rangle\}$ basis the relaxation operator reads

$$\mathcal{R}_\alpha^{00}{}_{n'_1 n'_2, n_1 n_2} = -\frac{1}{2} \delta_{n_1 n'_1} \sum_v \Lambda_+^\alpha(\omega_{n_2 v}) S_{n_2 v} S_{n'_2 v} - \frac{1}{2} \delta_{n_2 n'_2} \sum_v \Lambda_+^\alpha(\omega_{n_1 v}) S_{n_1 v} S_{n'_1 v} \quad (18a)$$

$$\mathcal{R}_\alpha^{11}{}_{v'_1 v'_2, v_1 v_2} = -\frac{1}{2} \delta_{v_1 v'_1} \sum_n \Lambda_-^\alpha(\omega_{n v_2}) S_{n v_2} S_{n v'_2} - \frac{1}{2} \delta_{v_2 v'_2} \sum_n \Lambda_-^\alpha(\omega_{n v_1}) S_{n v_1} S_{n v'_1} \quad (18b)$$

$$\mathcal{R}_\alpha^{01}{}_{n'_1 n'_2, v_1 v_2} = \frac{1}{2} \Lambda_-^\alpha(\omega_{n'_1 v_1}) S_{n_1 v_1} S_{n'_2 v_2} + \frac{1}{2} \Lambda_-^\alpha(\omega_{n'_2 v_2}) S_{n'_2 v_1} S_{n'_1 v_1} \quad (18c)$$

$$\mathcal{R}_\alpha^{10}{}_{v'_1 v'_2, n_1 n_2} = \frac{1}{2} \Lambda_+^\alpha(\omega_{n_1 v'_1}) S_{n_1 v'_1} S_{n_2 v'_2} + \frac{1}{2} \Lambda_+^\alpha(\omega_{n_2 v'_2}) S_{n_1 v'_1} S_{n_2 v'_2} \quad (18d)$$

$$\begin{aligned} \mathcal{R}_{B k'_1 k'_2, k_1 k_2}^{ii} &= \delta_{k'_2 k_2} \sum_k \gamma_+(\omega_{k'_1 k}^i) x_{k k_1}^i x_{k'_1 k}^i + \delta_{k'_1 k_1} \sum_k \gamma_-(\omega_{k k_2}^i) x_{k_2 k}^i x_{k k'_2}^i \\ &\quad + \gamma_+(\omega_{k'_1 k'_1}^i) x_{k'_1 k_1}^i x_{k_2 k'_2}^i + \gamma_-(\omega_{k'_2 k'_2}^i) x_{k_2 k'_2}^i x_{k'_1 k'_1}^i, \end{aligned} \quad (18e)$$

where we have introduced the following notation

$$\Lambda_+^\alpha(\omega_{nv}) = \Gamma_\alpha(\omega_{nv}) f_\alpha(\omega_{nv}), \quad (19a)$$

$$\Lambda_-^\alpha(\omega_{nv}) = \Gamma_\alpha(\omega_{nv}) [1 - f_\alpha(\omega_{nv})], \quad (19b)$$

$$\gamma_+(\omega_{k'k}) = 2\pi J(\omega_{k'k}) [1 + n_B(\omega_{k'k})], \quad (19c)$$

$$\gamma_-(\omega_{k'k}) = 2\pi J(\omega_{k'k}) n_B(\omega_{k'k}), \quad (19d)$$

with transition frequencies $\omega_{nv} = E_v^1 - E_n^0$ and $\omega_{kk'}^i = E_k^i - E_{k'}^i$ as well as transition elements $S_{m,v} = |\langle m, 0 | s(x) | v, 1 \rangle|^2$ and $x_{kk'}^i = |\langle k, i | x | k', i \rangle|^2$.

In the numerical calculations, the system Hamiltonian H_S is represented and diagonalized employing a discrete variable representation (DVR) method optimized for the double-well potential $V(x)$ using Hermite polynomials for the underlying grid.⁴² The stationary state of the reduced density matrix $\tilde{\rho} = \rho(t \rightarrow \infty)$ is obtained by solving the set of linear equations $\mathcal{L}\tilde{\rho} = 0$. The eigenstates employed for the representation of the density matrix ρ_{mn}^{ij} are truncated at $m, n = 60$. With this truncation, all localized states in the potential wells and a sufficient number of delocalized states above the energy barrier are included. To have a proper description of the observables of interest, the coherences of the density matrix have to be included in the calculation. To this end, we include the first six subdiagonals of the density matrix in both occupation spaces. Test calculations show that this provides converged results for the observables of interest.

The observables of interest comprise the current I , the probability distribution for the proton position $\rho(x)$ as well as the average position $\langle x \rangle$. The current is defined as the time derivative of the number of electrons in lead α ,

$$\hat{I}_\alpha = \frac{d}{dt} c_{k_\alpha}^\dagger c_{k_\alpha} = -ie [c_{k_\alpha}^\dagger c_{k_\alpha}, H] \quad (20)$$

which in the $\{|m, i\rangle\}$ basis reads

$$I_\alpha = \sum_{nv} \Gamma_\alpha(\omega_{nv}) S_{nv} \left[f_\alpha(\omega_{nv}) \sum_{n'} S_{n'v} \rho_{n'n}^{00} - [1 - f_\alpha(\omega_{nv})] \sum_{v'} S_{nv'} \rho_{vv'}^{11} \right]. \quad (21)$$

The probability distribution $\rho(x_\beta)$ for the proton position on the DVR grid $\{x_\beta\}$ is given by

$$\rho(x_\beta) = \sum_{i \in \{0,1\}} \sum_{n,m} \rho_{nm}^{ii} \phi_n^i(x_\beta) \phi_m^i(x_\beta) \Delta_\beta, \quad (22)$$

where $\phi_n^i(x_\beta)$ are the eigenfunctions of H_S in the DVR representation and Δ_β are the corresponding DVR weights. From this, the average position is straightforwardly obtained by the trace formula $\langle x \rangle = \text{Tr}_S(\hat{x}\rho)$.

We finally comment on the validity of the approximations used in this approach. The treatment of the molecule-reservoir coupling within second order perturbation theory limits the validity of the Redfield equations, Eq. (13), to sufficiently weak coupling between the system and the reservoirs. With respect to the molecule-lead coupling, co-tunneling effects

and broadening of features in the current-voltage characteristics are not included in this approximation. As a result, the validity of the approach requires temperatures with $k_B T \gg \frac{2\nu^2}{\gamma}$, a condition fulfilled in all calculations reported below. With respect to the coupling of the proton motion to the harmonic bath, the criterion for the validity of the approach is provided by the following condition for the relaxation tensor elements⁴³

$$\mathcal{R}_{B\mu\mu,\nu\nu}^{ii} \ll \omega_{\mu\nu}^i. \quad (23)$$

This criterion is fulfilled for the parameters considered below.

IV. RESULTS

The methodology outlined above is in the following applied to analyze the influence of intramolecular proton transfer on the conductance properties of a molecular junction. For this purpose, we consider the three model systems defined in table I corresponding to weak, medium and strong hydrogen bonding.

A. Weakly hydrogen bonded, high-barrier system

We first consider the system with weak hydrogen bonding and neglect the influence of the bias voltage on the potential $V_0(x)$ of the proton motion. This corresponds to a situation where the direction of the translocation path is parallel to the gate field (cf. Fig. 2), i.e. $\phi = \pi / 2$. The specific form of the double-well potential $V_0(x)$ depends thus only on the gate voltage U_g . For the choice $U_{g,\text{sym}} = \epsilon_0 d / (2l)$, the potential $V_0(x)$ is symmetric. This value of the gate voltage plays a special role (see below) and is in the following referred to as trigger point. For the subsequent discussion, it is useful to introduce the detuning voltage $U_d = U_g - U_{g,\text{sym}}$, which is a measure of the asymmetry of the potential $V_0(x)$. The global minimum of $V_0(x)$ is located in the left/right well for $U_d \lessgtr 0$. The influence of the bias voltage on the potential $V_0(x)$ is analyzed in Sec. IV A 4.

1. *Equilibrium properties*

To facilitate the analysis of the transport properties in Sec. IV A 3, we first discuss the equilibrium properties. Fig. 4 shows the potential $V_0(x)$ for three different choices of the detuning voltage, $U_d = -U_{g,\text{sym}}$ (ON), $U_d = 0.5$ V (OFFMIX) and $U_d = 1.3$ V (OFF),

where the labels in parenthesis are related to the transport properties (see below), and the respective eigenenergies and eigenstates. The potentials for the ON/OFF cases exhibit a pronounced asymmetry with a global minimum in the left/right well, while the case OFFMIX represents a potential that is closer to a symmetric double well. The spectra include localized states for energies below the barrier energy $V_b = 0.8$ eV and delocalized states above the barrier. For the specific parameters of $V_0(x)$ considered, there are eight states with energies below the barrier. This number is independent of the detuning voltage used. Furthermore, for asymmetric potentials, all states with energies below the minimum energy of the higher well are localized in the lower well, while states with energies above the minimum of the higher well come in pairs and may not be fully localized. In the following, the lowest-lying state of this class is referred to as the metastable state with energy E_m .

The details of the spectrum, such as the energy spacing, depend on the detuning voltage. In particular, the ground and the first excited state are well separated in energy for the ON and OFF system, while they are rather close for the OFFMIX system. Upon changing the detuning voltage, quasidegeneracies of the localized states occur, as illustrated in Fig. 5. We refer to these quasidegeneracies as resonances and denote the detuning voltage of the n -th resonance for positive (negative) detuning as U_n^+ (U_n^-). This classifies the OFF system as the first resonance with detuning voltage $U_d = U_1^+$ and the symmetric potential at the trigger point $U_d = 0$ as the zeroth resonance state.

The diamond pattern of the energies in Fig. 5 results from the oscillation of energies between adjacent states upon change of the detuning voltage. Specifically, a positive detuning ($U_d > 0$ V) lifts the energies of the states localized in the left well and lowers the energies of those localized in the right well. At the resonance $U_d = U_1^+$ (corresponding to the OFF system), all states but the ground state form tunneling pairs. Further detuning ($U_d > U_1^+$) moves the first excited state into the more stable well. In general, the spectra of localized states for detuning values $U_n^+ < U_d < U_{n+1}^+$ consist of $n+1$ states localized in the more stable well with energies lower than that of the metastable state (E_m) and $8 - (n+1)$ localized states with higher energies.

Fig. 6 shows the population of the lowest-lying eigenstates, ρ_{ii}^{00} for the molecular junction in equilibrium, i.e. at zero bias voltage. At the trigger point ($U_d = 0$ V) the two lowest-lying states of the tunneling pairs are almost equally populated. For small detuning voltages, mostly the ground and metastable states are populated. At the first resonance, the energy difference between the metastable and the next higher-lying excited state minimizes so that

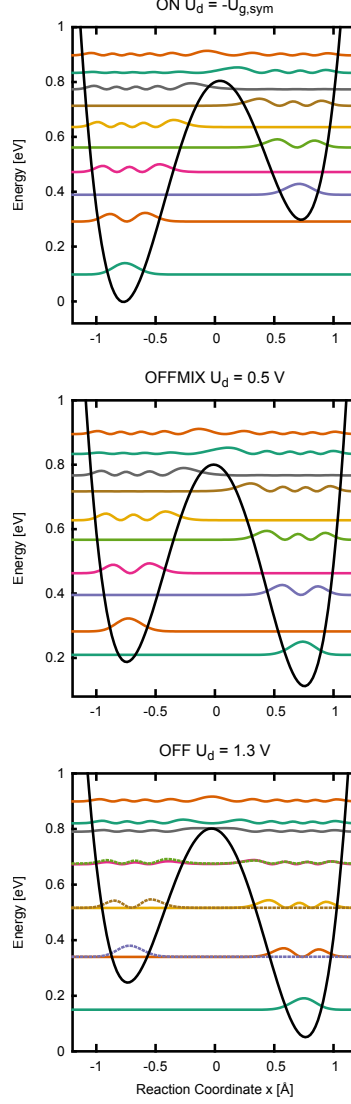


Figure 4. Potentials $V_0(x)$, spectra and density of the eigenfunctions of the weakly bonded system for different detuning voltages U_d .

their population becomes very similar although it is significantly smaller than that of the ground state.

2. *Elementary charge transfer processes*

The basic mechanism of electron transport in the molecular junction model considered in this work involves a sequence of two tunneling events. For positive bias, an electron with energy ε_{k_l} in the left lead tunnels onto the molecule and occupies the bridge state. Thereby, the proton is excited from the initial state $|n, 0\rangle$ to $|v, 1\rangle$ by energy exchange with the tunneling electron. We denote the corresponding process by $P_{n,v}$. In the subsequent

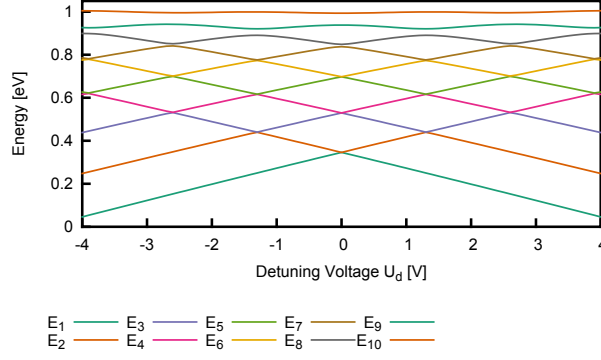


Figure 5. Eigenenergies of h_0 as a function of the detuning voltage.

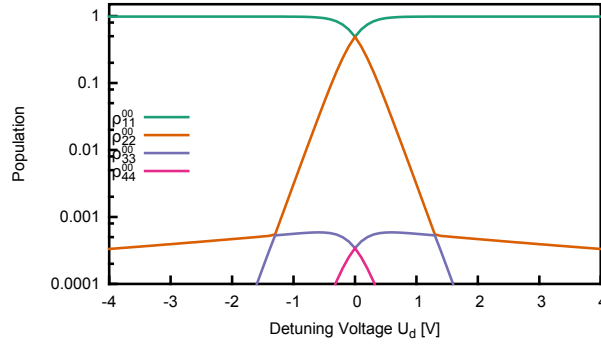


Figure 6. Populations of the lowest-lying eigenstates, ρ_{ii}^{00} , for the molecular junction in equilibrium with the leads.

event, the electron is transferred from the molecule to a state in the right lead with energy ε_{k_r} , accompanied by another transition of the proton

In the framework of Redfield theory, the energy is conserved within each individual process. The $P_{n,v}$ process defines a transport channel, which (for low temperatures $T \rightarrow 0$) is activated at threshold bias voltages $U_{nv} = \pm 2\omega_{nv}$, where the sign accounts for excitations (+) and deexcitations (-). For finite temperatures the thresholds are reduced due to thermal broadening of the lead states.

The threshold voltages U_{nv} are closely related to the energy spectra. This is illustrated for the OFFMIX system in Fig. 7, where the threshold voltages of the processes $P_{n,n+l} = P_l$ are shown. The blue vertical line at $U_{on} = 2\varepsilon_0 = 0.2$ V corresponds to the onset, where all elastic processes $P_{n,n}$ are enabled simultaneously. All other lines correspond to inelastic processes with $l > 0$.

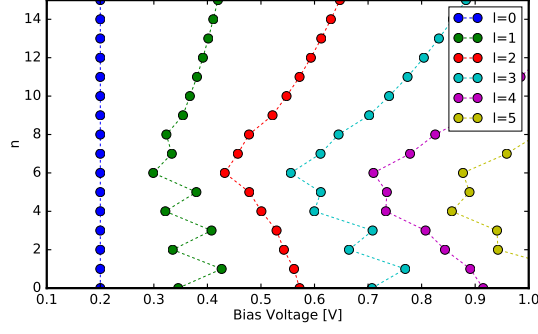


Figure 7. $P_{n,n+l}$ processes for the OFFMIX systems represented as points over the respective threshold voltages. Processes of equal l are depicted using the same color.

In a double well potential, transitions between localized states can be classified as intra- and inter-well transitions, which correspond in the OFFMIX system to processes with odd (e.g. $P_{n,n+1} = P_1$) or even (e.g. $P_{n,n+2} = P_2$) value of l , respectively. Fig. 7 demonstrates that the threshold voltages for the two types of processes follow different patterns. Inter-well processes P_1 exhibit for small n a zig-zag pattern, which is a result of the state pairing in the double well. Thereby, small threshold voltages correspond to transitions among pairs. On the other hand, the linear pattern for intra-well processes P_2 for small n is related to the decreasing energy gap between adjacent states localized in the same well. In particular, the energy differences are minimal around the barrier of the double-well potential. As a result, transport processes involving states close to the barrier are activated prior to those that involve states localized deeper in the potential well.

The analysis above has only considered the opening of the different transport channels. The extent to which open channels actually contribute to charge transport is determined by the nonequilibrium population of the states and the transition rates (cf. Eq. (18a)). The latter involve, besides the molecule-lead coupling, the transition elements $S_{m,v} = |\langle m, 0 | s(x) | v, 1 \rangle|^2$ with the switch function $s(x)$. The transition elements take the form

$$S_{m,v} = \left| \frac{1+\sigma}{2} \delta_{m,v} - \frac{1-\sigma}{2} \int dx \psi_v^1(x) \psi_m^0(x) \tanh(x) \right|^2, \quad (24)$$

where $\psi_k^i(x) = \langle x, i | \psi_k \rangle$.

For low bias voltages, transport is dominated by elastic processes P_0 involving localized states. For states strongly localized in the wells, the switch function $s(x)$ is nearly constant. In an asymmetric double-well potential, i.e. for $U_d \neq 0$, the transition elements for elastic

processes are obtained from Eq. (24) as $S_{m,m}^L \approx 1$ for the left and $S_{m,m}^R \approx \sigma^2$ for the right well, respectively. Thus, the rates of elastic processes in the right well are downscaled by a factor of σ^2 . On the other hand, for delocalized states, which are important for higher bias voltages, the wave functions can be assumed to be approximately constant, yielding for elastic transitions $S_{m,m}^D \approx (1 + \sigma)^2 / 4$.

Fig. 8 shows the transition elements for the inelastic processes P_1 as a function of the detuning voltage. The rates of these processes are rather small for lower-lying states due to the fact that these states localize in different potential wells. For higher-lying states, which become relevant at high energies/voltages, inelastic processes play a more significant role. The reason for this is that the wavefunctions of these states, which are mainly localized in one of the potential wells, exhibit also small tails in the other potential well. The contribution of these tails to the integral in Eq. (24) increases with higher energy, therefore enhancing the role of these processes. Furthermore, the transition elements of paired states can also give pronounced contributions resulting in the peaks depicted in Fig. 8, which occur at quasidegeneracies of the energies (see Fig. 5).

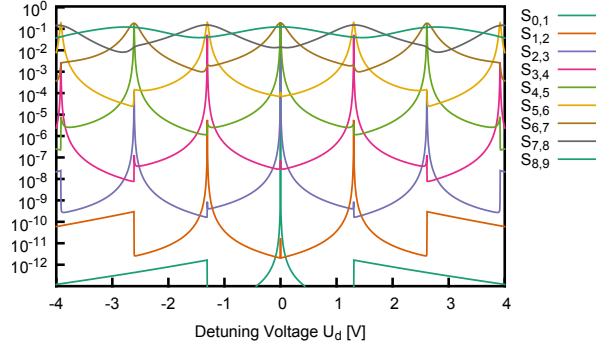


Figure 8. Transition elements $S_{n,n+1}$ of processes $P_{n,n+1}$ as a function of the detuning voltage

3. *Transport properties*

The current-voltage characteristics of the ON, OFFMIX, and OFF systems are shown in Fig. 9. For comparison, the current for the system without coupling between the electronic and proton degrees of freedom (in the following referred to as the uncoupled system) is also depicted. The currents of the coupled systems exhibit pronounced differences for small bias voltages but tend to the same saturation value of $I_{\text{sat}} = 0.4 \mu\text{A}$ for bias voltages

$U_b > U_{\text{sat}} = 1.5$ V, a value significantly smaller than that found for the uncoupled system. All coupled systems exhibit structures at low bias voltages, which are more pronounced for the OFF and OFFMIX systems. However, while in these systems the saturation current is approached from below, the ON system shows a more complex behavior. Specifically, this system exhibits a strong increase of the current at low bias voltages closely resembling that of the uncoupled system. This is followed by a plateau and a pronounced negative differential conductance (NDC) towards the saturation limit for larger bias voltages. In addition, the current of the ON system is always larger than that of the other two coupled systems.

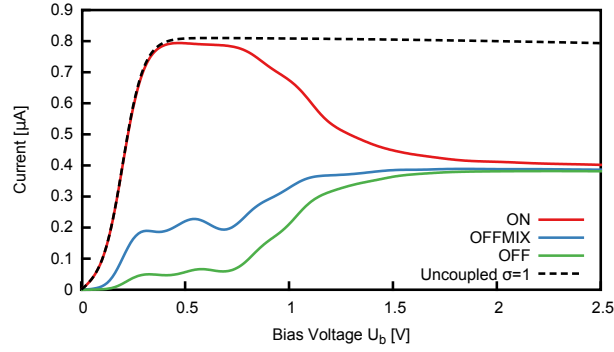


Figure 9. Current voltage characteristics of the ON, OFFMIX, OFF, and uncoupled ($\sigma = 1$) systems.

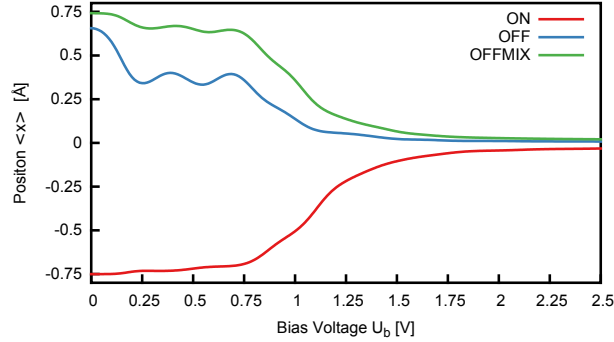


Figure 10. Average position of the proton $\langle x \rangle$ as a function of the bias voltage for the ON, OFF, and OFFMIX systems.

The behavior of the current-voltage characteristics can be rationalized on the basis of the position of the proton. Fig. 10 depicts the average position of the proton ($\langle x \rangle$) for the ON, OFFMIX, and OFF systems and Fig. 11 shows the probability distribution of the proton

($\rho(x)$) for the case of the OFFMIX system. At a given bias voltage U_b , the position of the proton determines the effective molecular-lead coupling via the switch function $s(x)$, cf. Eq. (9). As shown in Fig. 10 the average position of the proton for the three coupled systems resembles the overall behavior of the current-voltage characteristics. Specifically, an increase of the bias voltage drives the average position of the proton from the equilibrium position in one of the wells at $U_b = 0$ to the center of the double well potential $x_{\text{sat}} = 0$ Å at $U_b > 1.5$ V, indicating that it is fully delocalized.

A more detailed inspection of the average position of the proton as a function of the bias voltage shows that for low bias voltages, the proton remains localized at the global minimum in the ON and OFF systems, with the elastic transition $P_{1,1}$ of the ground state of the proton being the dominant contribution to the transport process. Since the transition element for the localization in the left well is $S_{1,1}^L \approx 1$, the effective molecule-lead coupling of the ON system corresponds to that of the uncoupled case ($\sigma = 1$). This explains the similarities found in the conductance of both systems in the range of bias voltages $U_b < 0.5$ V. In contrast, due to the localization of the proton in the right well, the molecule-lead coupling in the OFF system is downscaled by a factor of $S_{1,1}^R / S_{1,1}^L \approx \sigma^2 \approx 0.01$, which agrees with the observed ratio of the currents in the ON/OFF systems.

In the case of the OFFMIX system, in addition to the ground state the metastable state is also significantly populated at $U_b = 0$ V as discussed in Sec. IV A, which shifts the equilibrium position of the proton slightly towards x_{sat} . As a result, the current at low bias voltages in this system involves contributions of the ground state process $P_{1,1}$ and the metastable state process $P_{2,2}$ resulting in values of the current that are between those of the ON and OFF systems.

At bias voltages larger than the onset value of $U_{\text{on}} = 0.2$ V, excited vibrational states are populated. In the ON system, the first vibrational excited state is located in the same well as the ground state. As a result, the excitation of this state hardly changes the position of the proton and the molecule-lead coupling and the current remains at a plateau. In contrast, this situation is reversed in the OFFMIX case and, as a result, the position of the proton changes notably in this system, as shown by the redistribution of population among the two wells in Fig. 11.

For higher bias voltages $U_b > U_{\text{on}}$, inelastic transport processes are activated. In the OFFMIX system, these processes result in pronounced oscillations of the average position and the current as a function of the bias voltage. As discussed in Sec. IV A 2, these oscilla-

tions are related to contributions of the inelastic processes $P_{n,n+1}$ and $P_{n,n+2}$. The ON and OFF systems also exhibit oscillatory structures in this bias voltage range, but these are less pronounced due to the more localized character of the states populated.

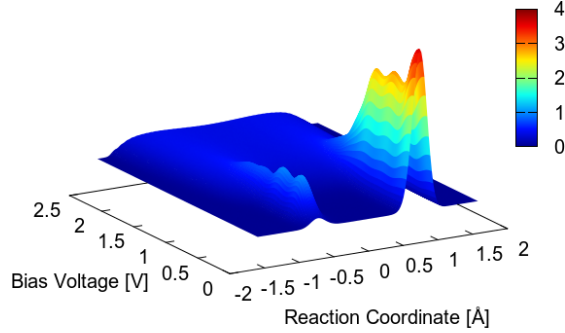


Figure 11. Probability distribution of the proton position $\rho(x)$ as a function of the bias voltage for the OFFMIX system.

Increasing the bias voltage further towards the saturation value $U_{\text{sat}} \approx 1.5$ V, activates inelastic processes that excite the proton above the barrier. In particular, transitions from localized to delocalized states close to the potential barrier become important. As a result, the proton is distributed almost uniformly over the translocation path as shown in Fig. 11 for the OFFMIX system (a similar result is found for the ON and OFF systems) leading to an average position of $\langle x \rangle = 0$ Å. Since in this voltage range the accesible vibrational states are populated almost equally, the effective molecular-lead coupling is given by the average of the switching function, $\int_{-\infty}^{\infty} s(x)dx = \frac{1+\sigma}{2} \approx 0.5$. This result explains the reduction of the current of the ON system from the plateau value to the saturation value corresponding to a pronounced NDC behavior. Based on this reasoning, any system with a detuning voltage of $U_d < 0$ V is expected to show this qualitative behavior.

The results discussed so far demonstrate that employing a gate voltage different conductance states of the molecular bridge in the junction can be achieved exhibiting low current (OFF system) or high current (ON system). This is, however, restricted to a certain range of bias voltages. For high bias voltages, the ability to control the conductance state of the molecular bridge in the junction using the gate potential is lost because delocalized states above the barrier are populated. However, the control of the conductance state of the molecular bridge in the junction can be recovered if the relaxation of the proton motion

due to interaction with other vibrational modes of the molecule, phonons in the electrodes or solvent is taken into account.

Fig. 12 shows the current-voltage characteristics of the ON, OFF, and OFFMIX systems including relaxation of the proton motion. This effect was modeled by coupling the system to a harmonic bath, Eq. (10) with coupling strength $\eta = 0.001$ corresponding to weak coupling. For comparison, the current of the system without coupling between the electronic and proton degrees of freedom ($\sigma = 1$) is also depicted.

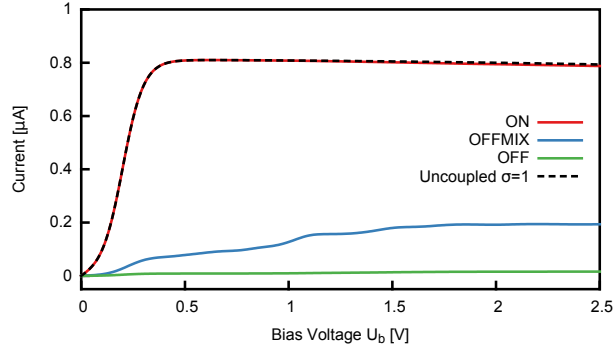


Figure 12. Current-voltage characteristics of the ON, OFFMIX, and OFF systems calculated including the coupling to a harmonic bath ($\eta = 0.001$). For comparison, the current of the system with no coupling between the electronic and proton degrees of freedom ($\sigma = 1$) is also shown.

The results in Fig. 12 show that for the three systems the current is different over the whole range of bias voltages. This result, which differs from that obtained in the absence of a system-bath coupling (see Fig. 9), is a consequence of the relaxation of the proton motion, which results in the population of low-lying, localized states even for large voltages. This is demonstrated in Fig. 13 for the probability distribution of the proton position $\rho(x)$ of the OFFMIX system. A detailed analysis of the transition elements $X_{k,k'}$ of the harmonic bath reveals that the relaxation is most effective among delocalized states and states localized in the same well below the barrier.

4. *Functionality*

The dependence of the current on the gate voltage can be utilized to realize a molecular transistor. This is demonstrated in Fig. 14, which shows the current as a function of the detuning voltage for a fixed bias voltage $U_b = 0.7$ V. This value ensures that even without

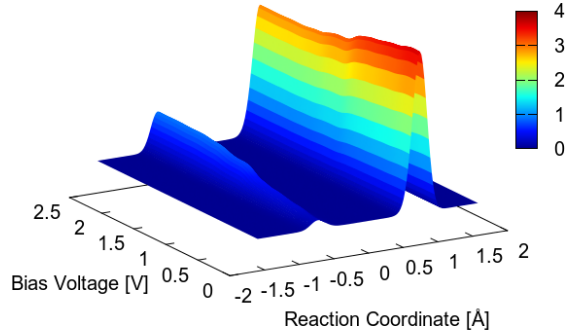


Figure 13. Probability distribution of the proton position $\rho(x)$ of the OFFMIX system calculated for a system-bath coupling of $\eta = 0.001$.

relaxation (i.e. $\eta = 0$), the proton is localized in one of the wells. The results show a transition from a high current (“ON”) to a low current (“OFF”) state at a detuning voltage $U_d \sim 1 - 2$ V indicating the translocation of the proton. This transition voltage is slightly off the expected value of $U_d = 0$. This is due to the different contribution of elastic processes in the left and right wells. Although the population of the uplifted left well decreases with the increase of the detuning voltage $U_d > 0$ V, the corresponding weaker transport processes in this well have a pronounced impact on the current since their contribution is enhanced by a factor of $1/\sigma^2 = 100$. In the reverse situation for $U_d < 0$ V, the transport processes in the uplifted right well are negligible owing to this factor. Therefore the current saturates asymmetrically with respect to the trigger point.

Coupling to the harmonic bath results in a shrinking of the transition zone because the bath suppresses the population of the metastable state as it facilitates the relaxation of the proton to the ground state. This results in a defined conductance state already at small detuning voltages. The current also exhibits structures at certain detuning voltages (see Fig. 14) which, as discussed in Sec. IV A 2, correspond to the U_n resonances.

So far, we have neglected the effect of the bias voltage on the proton potential, corresponding to a value of $\phi = \pi/2$ (cf. Eq. 5). In the following, we study the more general case and show that the influence of the bias voltage on the proton potential results in a diode-like behavior of the molecular junction. For a general angle ϕ and a given gate voltage U_g , the bias voltage at which the potential for the intramolecular proton transfer is a symmetric

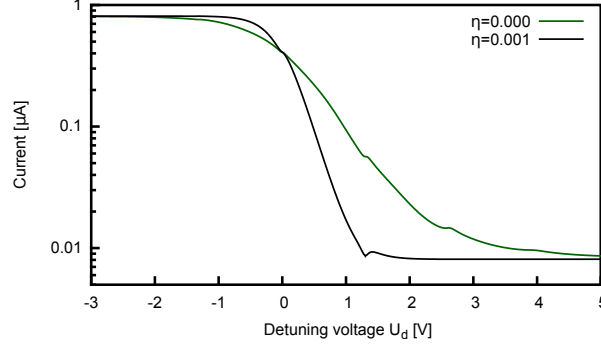


Figure 14. Current as a function of the detuning voltage U_d for a constant bias voltage $U_b = 0.7$ V with and without system-bath coupling (η). At a detuning voltage $U_d \sim 1 - 2$ V the “ON” state switches to the “OFF” state.

double well (the so-called trigger point) is given by

$$U_{b,\text{sym}}(U_g) = \frac{L_m \varepsilon_d}{2l \cos(\varphi)} - \frac{L_m}{d} U_g \tan(\varphi). \quad (25)$$

Therefore, the global minimum of the potential is located in the left well for $U_b < U_{b,\text{sym}}$ and otherwise in the right well.

Fig. 15 shows the current-voltage characteristics for an angle of $\phi = \pi / 4$, system-bath coupling $\eta = 0.001$ and for different values of the gate potential corresponding to different trigger points, $U_{b,l}(3.2) = -0.37$ V, $U_{b,r}(2.5) = 0.32$ V and $U_{b,c}(2.82) = 0$ V. The current-voltage characteristics shows the typical behavior of a diode with a significant current for negative bias voltages and vanishing current for large positive bias voltages. The details depend on the chosen gate voltage and, as a consequence, on the trigger point.

As shown in Fig. 15, all systems considered exhibit a NDC effect for positive bias voltages, which is most pronounced for the system with the trigger point located at $U_b = U_{b,r}$. This system corresponds to an “ON” conductance state for the bias voltage $U_b \leq U_{b,r}$ resulting in a high current at the onset of the positive bias. For larger bias voltages $U_b \geq U_{b,l}$ the current decreases since the “OFF” state stabilizes and becomes increasingly populated. Although the effect is similar to that found for the ON system discussed in Sec.IV A 3 the cause of the NDC in this case does not relate to the reduction of the effective molecular-lead coupling as a consequence of the delocalization of the proton but rather to the change of the global minima. The rise of the current at positive voltages is less pronounced in the system with the trigger point at $U_{b,l}$. In this system, the conductance state is already changed to “OFF” at $U_b = U_{b,l}$ before the bias voltage becomes positive, which results in a smaller current. In

conclusion, the position of the trigger point $U_{b,\text{sym}}$ determines the increase in the current at positive bias voltages due to contributions of the transport processes in the left well, which cause a significant enhancement of the current. For larger bias voltages the contribution of these processes decreases as a consequence of the destabilization of the left potential well.

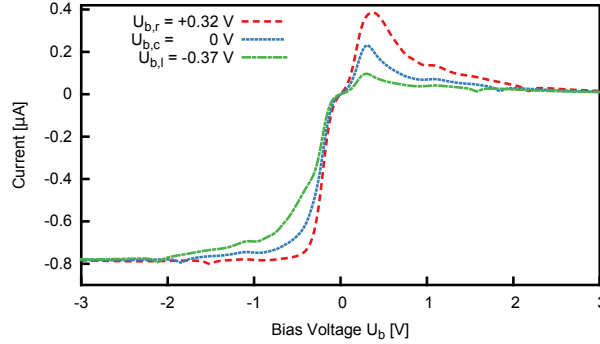


Figure 15. Current-voltage characteristics for different values of the gate potential (see text) corresponding to different trigger points and for a system bath coupling $\eta = 0.001$ calculated for an angle $\phi = \pi / 4$ between the proton translocation path and the bias field.

B. Stronger hydrogen bonded, low-barrier systems

In this section, we expand our analysis and consider systems with smaller barriers for the intramolecular proton transfer reaction and stronger hydrogen bonding. Specifically, we consider two representative systems with the potentials shown in Fig. 16. The parameters are given in table I. For simplicity, in this section we neglect the influence of the bias voltage on the potential $V_0(x)$ of the proton motion. This corresponds to a situation, where the direction of the translocation path is parallel to the gate field (cf. Fig. 2), i.e. $\phi = \pi / 2$.

1. *Equilibrium properties*

The energy spectra and character of the eigenstates of the two strongly bonded systems shown in Fig. 16 differ significantly from those of the weakly bonded system considered in Sec. IV A. Specifically, in the medium bonded system, only two localized states exist with energies below the barrier. In the strongly bonded system already the ground state has an energy above the very small barrier and thus no localized eigenstates exist. The trigger

points of the medium and the strongly bonded system are $U_{g,\text{sym}}^m = 1.0$ V and $U_{g,\text{sym}}^s = 0.5$ V.

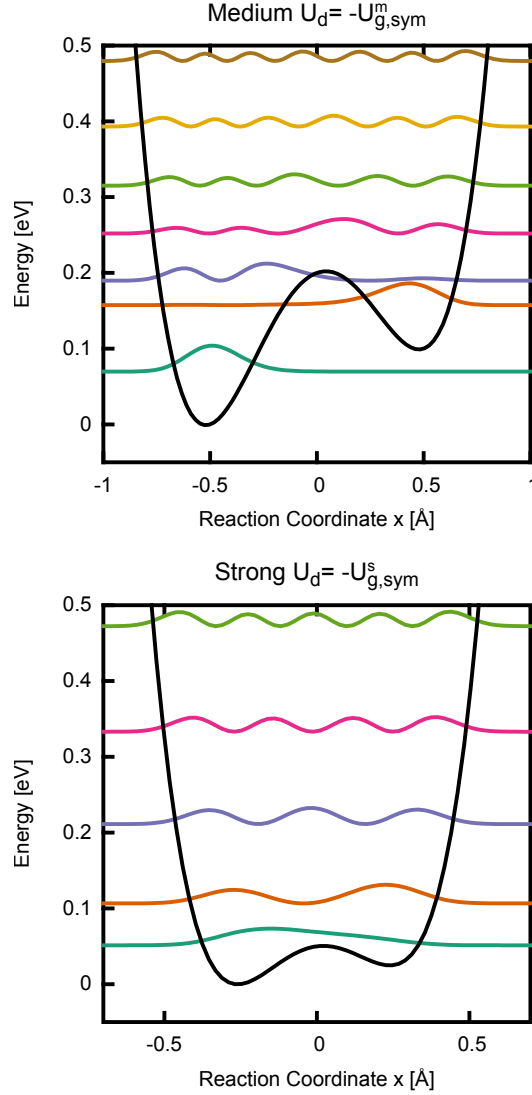


Figure 16. Potentials $V_0(x)$, spectra and density of the eigenfunctions of the medium and strongly hydrogen bonded systems.

As a consequence, the localization of the proton in the equilibrium state is also quite different in the three systems, as indicated by the probability of finding the proton in the right half-space, $T_R = \int_0^\infty \rho(x)dx$, depicted in Fig. 17 as a function of the gate voltage U_g . At their respective trigger points, the proton is equally distributed, $T_R = 0.5$, owing to the symmetry of the potentials. While the weakly and medium bonded system exhibit a rather sharp transition between wells, in the strongly bonded system it is spread over a large range of gate voltages. This is due to the fact that this system has no localized states at the trigger

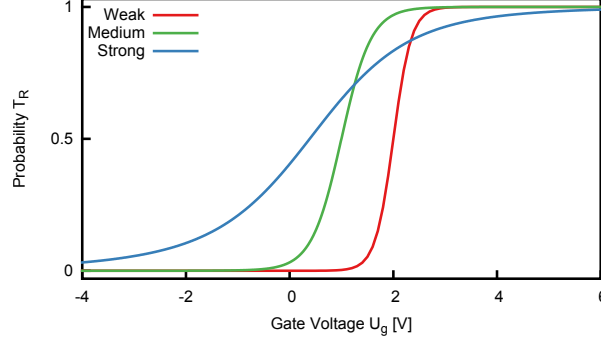


Figure 17. Probability of finding the proton in the right half-space (T_R) as a function of the gate voltage for the three systems corresponding to weak, medium, and strong hydrogen bonding.

point and thus a relatively large gate voltage is required to achieve localization in one of the wells.

2. *Transport properties*

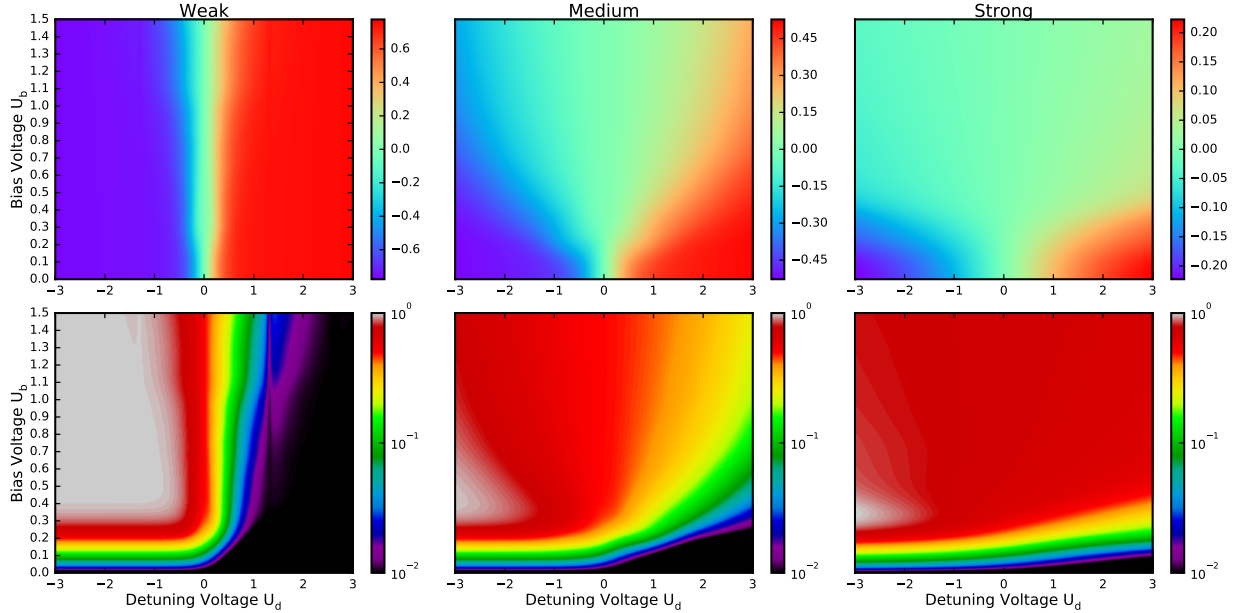


Figure 18. Average position $\langle x \rangle$ (top) and corresponding current ratio I / I_{max} (bottom) as a function of detuning and bias voltage for the three systems corresponding to weak, medium, and strong hydrogen bonding. The results have been obtained including a system-bath coupling with strength $\eta = 0.001$.

Fig. 18 shows the average proton position $\langle x \rangle$ (upper panels) and the current (lower panels) as a function of the detuning and bias voltage for the weakly, medium, and strongly bonded systems. The results have been obtained taking relaxation of the proton into account ($\eta = 0.001$). For better comparability, the current is shown relative to its maximal value, which is given by $I_{max}^w = I_{max}^m = 0.81 \mu A$ and $I_{max}^s = 0.59 \mu A$ for the weakly, medium, and strongly bonded system, respectively.

The results for the average proton position show clearly the regions of localization in the left (blue) and the right (red) well. These regions are separated by the funnel-shaped region of delocalization (green) centered at the trigger point. The shape of this region is quite different for the three systems investigated. Specifically, in the weakly bonded system the proton is localized for most detuning and bias voltages and the delocalization region extends over a narrow range of small detuning voltages corresponding to a symmetric double-well potential. In the more strongly bonded systems, on the other hand, the proton is always delocalized for sufficiently high bias voltages.

As a result of the distinct localization pattern exhibited by the proton for the different systems, their current-voltage characteristics differ significantly. While the weakly bonded system shows a distinct dependence of the current on the detuning voltage, this is less pronounced in the medium bonded system and almost negligible in the strongly bonded system. As a consequence, only the weakly bonded system, which exhibits a significant barrier, can fulfill the functionalities of a transistor or a diode.

V. CONCLUSIONS

In this paper we have studied the influence of an intramolecular proton transfer reaction on the conductance of a molecular junction. To this end, we have used a generic model for a proton transfer reaction with parameters motivated by our previous first-principles studies and employed a quantum master equation approach at the level of Redfield theory to solve the transport problem.

The results show that it is possible to control the conductance state of molecular junctions using a proton transfer reaction in combination with external electric fields. Depending on the location of the proton, the junction exhibits high or low current. Considering different parameter regimes, which range from weak to strong hydrogen bonding and include situations with high or low barriers separating the reactant and product of the reaction, we have identified necessary preconditions for achieving control. We have also demonstrated that

the proton transfer mechanism can be utilized to achieve functionality. Employing external fields of a gate or the lead electrodes, the current-voltage characteristics of the molecular junction in systems with a weak hydrogen bond and a significant energy barrier for the proton transfer resemble those of a transistor or a molecular diode.

In the present paper, we have used a generic model and focused on the steady state transport properties. Another interesting question concerns the time-dependent transport properties, e.g. how the steady state of the molecular junction is reached. For a realization of a molecular switch, for example, an intriguing question is how the low conductance state transforms into the high conductance state and vice versa upon change of the external electric field. This question, as well as an extension of the model towards a first-principles based description will be the topic of future investigations.

ACKNOWLEDGMENTS

We thank Ivan Pshenichnyuk and Andrzej Sobolewski for helpful and inspiring discussions. This work has been supported by the German-Israeli Foundation for Scientific Development (GIF) and the German Research Foundation (DFG) through the Cluster of Excellence 'Engineering of Advanced Materials' (EAM), SFB 953 and a research grant. Generous allocation of computing time at the computing centers in Erlangen (RRZE) and Munich (LRZ) is greatly acknowledged.

REFERENCES

- ¹G. Cuniberti, G. Fagas, and K. Richter, *Introducing Molecular Electronics* (Springer, Heidelberg, 2005).
- ²J. C. Cuevas and E. Scheer, *Molecular Electronics: An Introduction to Theory and Experiment* (World Scientific Publishing Co. Pte. Ltd., Singapore, 2010).
- ³N. A. Zimbovskaya and M. R. Pederson, Phys. Rep. **509**, 1 (2011).
- ⁴J. Bergfield and M. Ratner, Phys. Status Solidi B **250**, 2249 (2013).
- ⁵I. Baldea, *Molecular Electronics: An Experimental and Theoretical Approach* (Pan Stanford, Singapore, 2015).
- ⁶D. Xiang, X. Wang, C. Jia, T. Lee, and X. Guo, Chem. Rev. **116**, 4318 (2016).
- ⁷A. Aviram and M. Ratner, Chem. Phys. Lett. **29**, 277 (1974).

- ⁸M. Elbing, R. Ochs, M. Koentopp, M. Fischer, C. von Hänisch, F. Weigend, F. Evers, H. B. Weber, and M. Mayor, *Proc. Natl. Acad. Sci. U. S. A.* **102**, 8815 (2005).
- ⁹E. Lörtscher, B. Gotsmann, Y. Lee, L. Yu, C. Rettner, and H. Riel, *ACS Nano* **6**, 4931 (2012).
- ¹⁰B. Capozzi, J. Xia, O. Adak, E. J. Dell, Z.-F. Liu, J. C. Taylor, J. B. Neaton, L. M. Campos, and L. Venkataraman, *Nature Nanotech* **10**, 522 (2015).
- ¹¹H. Park, J. Park, A. K. L. Lim, E. H. Anderson, A. P. Alivisatos, and P. L. McEuen, *Nature* **407**, 57 (2000).
- ¹²M. Perrin, E. Burzuri, and H. van der Zant, *Chem. Soc. Rev.* **44**, 902 (2015).
- ¹³S. van der Molen and P. Liljeroth, *J. Phys. Cond. Mat.* **22**, 133001 (2010).
- ¹⁴Z. Donhauser, B. Mantooth, K. Kellyand, L. Bummand, J. Monnelland, J. Stapleton, D. Price, A. Rawlett, D. Allara, J. Tour, and P. Weiss, *Science* **292**, 2303 (2001).
- ¹⁵F. Morescoand, G. Meyer, K.-H. Rieder, H. Tang, A. Gourdon, and C. Joachim, *Phys. Rev. Lett.* **86**, 672 (2001).
- ¹⁶D. Dulic, S. van der Molen, T. Kudernac, H. Jonkman, J. de Jong, T. Bowden, J. van Esch, B. Feringa, and B. van Wees, *Phys. Rev. Lett.* **91**, 207402 (2003).
- ¹⁷J. Li, G. Speyer, and O. Sankey, *Phys. Rev. Lett.* **93**, 248302 (2004).
- ¹⁸P. M. Mendes, A. H. Flood, and J. F. Stoddart, *Appl. Phys. A* **80**, 1197 (2005).
- ¹⁹B.-Y. Choi, S.-J. Kahng, S. Kim, H. Kim, H. Kim, Y. Song, J. Ihm, and Y. Kuk, *Phys. Rev. Lett.* **96**, 156106 (2006).
- ²⁰M. del Valle, R. Gutierrez, C. Tejedor, and G. Cuniberti, *Nature Nanotech.* **2**, 176 (2007).
- ²¹P. Liljeroth, J. Repp, and G. Meyer, *Science* **317**, 1203 (2007).
- ²²C. Benesch, M. Rode, M. Cizek, R. Härtle, O. Rubio-Pons, M. Thoss, and A. Sobolewski, *J. Phys. Chem. C* **112**, 9880 (2008).
- ²³S. Pan, Q. Fu, T. Huang, A. Zhao, B. Wang, Y. Luo, J. Yang, and J. Huo, *Proc. Natl. Acad. Sci. USA* **106**, 15259 (2009).
- ²⁴W. Auwärter, K. Seufert, F. Bischoff, D. Eciija, S. Vijayaraghavan, S. Joshi, F. Klappenberger, N. Samudrala, and J. Barth, *Nature Nanotech.* **7**, 41 (2011).
- ²⁵P. Zhao, P. Wang, Z. Zhang, and D. Liu, *Physica B* **405**, 446 (2010).
- ²⁶C. Hofmeister, R. Härtle, O. Rubio-Pons, P. B. Coto, A. L. Sobolewski, and M. Thoss, *J. Mol. Model.* **20**, 1 (2014).
- ²⁷J. Jankowska, J. Sadlej, and A. L. Sobolewski, *Phys. Chem. Chem. Phys.* **17**, 14484 (2015).

- ²⁸M. Cizek, M. Thoss, and W. Domcke, Czech. J. Phys. **55**, 189 (2005).
- ²⁹J. Koch, M. Semmelhack, F. von Oppen, and A. Nitzan, Phys. Rev. B **73**, 155306 (2006).
- ³⁰A. Donarini, M. Grifoni, and K. Richter, Phys. Rev. Lett. **97**, 166801 (2006).
- ³¹I. Pshenichnyuk and M. Cizek, Phys. Rev. B **83**, 165446 (2011).
- ³²L. Kecke and J. Ankerhold, Phys. Rev. B **85**, 245442 (2012).
- ³³A. Dzhioev, D. Kosov, and F. von Oppen, J. Chem. Phys. **138**, 134103 (2013).
- ³⁴R. Pozner, E. Lifshitz, and U. Peskin, Nano Lett. **14**, 6244 (2014).
- ³⁵G. R. Desiraju and T. Steiner, *The Weak Hydrogen Bond: In Structural Chemistry and Biology* (Oxford University Press, 2001).
- ³⁶R. H. McKenzie, C. Bekker, B. Athokpam, and S. G. Ramesh, J. Chem. Phys. **140**, 174508 (2014).
- ³⁷C. L. Perrin and J. B. Nielson, Annu. Rev. Phys. Chem. **48**, 511 (1997).
- ³⁸M. Cizek, M. Thoss, and W. Domcke, Phys. Rev. B **70**, 125406 (2004).
- ³⁹U. Peskin, J. Phys. B: At. Mol. Opt. Phys. **43**, 153001 (2010).
- ⁴⁰C. Timm, Phys. Rev. B **77**, 195416 (2008).
- ⁴¹A. Nitzan, *Chemical Dynamics in Condensed Phases: Relaxation, Transfer and Reactions in Condensed Molecular Systems* (Oxford University Press, Oxford, 2006).
- ⁴²R. G. Littlejohn, M. Cargo, T. C. Jr, K. A. Mitchell, and B. Poirier, J. Chem. Phys. **116**, 8691.
- ⁴³D. Egorova, M. Thoss, W. Domcke, and H. Wang, J. Chem. Phys. **119**, 2761 (2003).